



OPEN UV-assisted fluctuation-enhanced gas sensing by ink-printed MoS₂ devices

Katarzyna Drozdowska¹✉, Janusz Smulko¹, Jakub Czubek¹, Sergey Rummyantsev² & Andrzej Kwiatkowski¹

In this work, MoS₂ flakes were printed on ceramic substrates and investigated toward 1–10 ppm of nitrogen dioxide (NO₂), 2–12 ppm of ammonia (NH₃), and 2–12 ppm acetone (C₃H₆O) under UV light (275 nm). The structure of overlapping MoS₂ flakes and UV light assistance affected high responsivity to NO₂ when DC resistance was monitored, and superior sensitivity to NH₃ was obtained from the low-frequency noise spectra. MoS₂ exhibited response and recovery times in hundreds of seconds and stability throughout the experiments conducted within a few months. MoS₂ sensor exhibited a resistance drift during the detection of a specific relaxation time. Subtracting the baseline burden with exponential drift exposed the direction of changes induced by oxidizing and reducing gases and reduced DL to 80 ppb, 130 ppb, and 360 ppb for NO₂, NH₃, and C₃H₆O, respectively. The fluctuation-enhanced sensing (FES) revealed that the adsorption of NO₂ on MoS₂ decreases the noise intensity, whereas adsorbed NH₃ increases the fluctuations of current flowing through the sensor, and these changes are proportional to the concentration of gases. The noise responses for NO₂ and NH₃ were opposite and higher than DC resistance responses with subtracted baseline (an increase of 50% for 10 ppm of NO₂ and an increase of more than 600% for 12 ppm of NH₃), showing that FES is a highly sensitive tool to detect and distinguish between these two gases. This way, we introduce a simple and low-cost method of gas sensor fabrication using ink-printed MoS₂ and the possibility of enhancing its sensitivity through data processing and the FES method.

The unique electronic, optical, and structural properties of various two-dimensional (2D) materials are attractive to researchers from different fields of science and explored for manufacturing field-effect transistors (FETs), solar cells, supercapacitors, and photodetectors¹. The structure of bulk MoS₂ consists of 2D S-Mo-S layers attracted to each other by weak van der Waals forces. Due to this fact, similarly to graphene, MoS₂ can be easily exfoliated to its 2D form. 2D MoS₂ usually exhibits *n*-type conductivity; however, depending on the synthesis process or if it forms a junction with other materials, it can also act as a *p*-doped semiconductor^{2,3}. Monolayered MoS₂ is characterized by attractive structural and transport properties, including large specific surface area and surface activity, as well as high carrier mobility, which is beneficial compared to other gas-sensitive materials such as pure metal oxides or polymers. At the same time, gas sensors based on the pristine form of this material can exhibit limited selectivity and extended sensing response and recovery time, which is unfavorable in gas detection and still requires fixing⁴. Still, the optoelectronic properties of MoS₂ attract great attention for light-assisted gas sensing, as the bandgap of MoS₂ (and other TMDCs as well) depends on a number of monolayers and enables tuning of their electrical properties with light, which is not possible in graphene⁵. The monolayered MoS₂ has a direct bandgap of ~ 1.8–1.9 eV, which falls in the red-light range (~ 660–690 nm). Because of that, some reports on light-assisted gas sensing by monolayered MoS₂ focus on detection enhanced by red light, which generates extra charge carriers participating in molecular adsorption⁶. The mechanisms of gas adsorption/desorption by mono- or a few-layered MoS₂ confirmed by theoretical computations and experimental works are well summarized elsewhere^{7,8}. In the case of organic vapors, their detection is limited due to the poor carrier exchange between the molecules and the sensing layer. Thus, e.g., sensing traces of acetone (sub-ppm concentrations) usually requires elevated operating temperatures, which also facilitates detection in humid conditions^{9–11}.

The gas-sensing properties of MoS₂ can be enhanced by different means, mainly to improve the sensor response and recovery times, sensitivity, and selectivity^{12,13}. Doping with noble metals or metal oxides^{2,14}, forming a junction with other nanomaterials¹⁵, elevated temperatures, and visible or UV light assistance^{6,16} were

¹Department of Metrology and Optoelectronics, Faculty of Electronics, Telecommunications, and Informatics, Gdańsk University of Technology, G. Narutowicza 11/12, 80-233 Gdańsk, Poland. ²Institute of High Pressure Physics PAS, CENTERA Laboratories, Warsaw, Poland. ✉email: katarzyna.drozdowska@pg.edu.pl

tested by numerous research groups. For instance, selectivity to NO_2 was obtained when MoS_2 was irradiated with UV light¹⁷. However, the method of fluctuation-enhanced sensing (monitoring low-frequency noise spectra) was also utilized to increase the selectivity of MoS_2 -based sensors to organic vapors such as chloroform, tetrahydrofuran, acetonitrile, and acetone¹⁸. The random resistance component can be highly informative about the surface processes of gas adsorption. Fluctuation-enhanced sensing (FES) utilizes low-frequency noise spectra as a sensitive tool for gas detection. The flicker noise ($1/f$ noise) can be affected by molecular adsorption due to the transfer of charges, resulting in fluctuations in their concentration and mobility¹⁹. The adsorption of molecules can result in a change in the noise intensity but also in the shape of the spectra (change in the slope due to induction of dominant generation-recombination events that produce the Lorentzians of characteristic frequencies). Until now, FES was successfully applied to distinguish between organic vapors by graphene back-gated FET or to determine the concentration of NO_2 by networks of carbon nanotubes^{20,21}. Thus, the method can potentially be a highly sensitive tool for devices based on other low-dimensional materials, including MoS_2 . Since FES has not been applied to layers of 2D semiconducting flakes, our studies fill a research gap for energy-efficient gas sensors with high potential for practical applications^{22–24}.

Since high-performance room-temperature gas detection remains an open issue for devices based on low-scale structures, light-activated sensors attract great attention. On the one hand, quanta of the visible light carry enough energy to generate electron-hole pairs and induce photoconductivity²⁵. Increasing the current flowing through the sensor is essential for any practical applications since MoS_2 layers are usually of high resistance. On the other hand, UV light activates the material surface by partly desorbing oxygen species and humidity and creating weakly bonded oxygen ions (oxygen photoions) that can be easily replaced by target gas molecules during detection²⁶, so it can stabilize and enhance sensing responses and secure photodesorption during recovery by shortening its time.

For fabricating sensors that rely on 2D materials, additive manufacturing has recently become an intriguing approach^{27,28}. In the case of printed MoS_2 -based gas sensors, Yao et al. showed promising sensitivity toward 5 ppm of NH_3 at room temperature in 2013²⁹. Simultaneously, the authors highlighted that the sensor needs further optimization due to the long response and recovery times. In the case of NO_2 and NH_3 sensing shown by Chen et al.³⁰, the detection limit in the ppb range was obtained for a single MoS_2 flake, but at 100 V bias. Thus, reducing the energy consumption for printed MoS_2 -based sensor operation still requires investigation. Nevertheless, the easy and low-cost fabrication of printed MoS_2 and its attractive optoelectronic properties hold a promise for high-quality performance as light-enhanced gas sensors. This approach solves the practical problem of proposing low-cost gas sensors of reduced energy consumption.

Herein, we studied the optical properties of the MoS_2 flakes dispersion and MoS_2 -based sensor responses toward three gases, representing different types of species and interactions with low-dimensional MoS_2 , namely nitrogen dioxide (NO_2), ammonia (NH_3), and acetone ($\text{C}_3\text{H}_6\text{O}$). We aim to propose a simple fabrication method of producing MoS_2 -based sensors and post-processing the obtained responsivity data to enhance the sensitivity and provide sensors of low detection limits at RT. We also utilize the FES method and show that the intensity of fluctuations generated in the MoS_2 sensor depends on the type and concentration of the selected gases, which increases the selectivity of such sensors. This way, we point toward a reproducible and easy method of producing and measuring gas sensing devices based on 2D materials and sensing data analysis.

Methods

MoS_2 sensors fabrication

MoS_2 flakes dispersed in ethanol-water solution (flakes concentration of 18 mg/L) were purchased from Graphene Supermarket. According to the producer, MoS_2 flakes are of 100–400 nm lateral size and thickness of 1–8 monolayers. The structural and optical characteristics of MoS_2 flakes, including SEM and AFM images, UV-Vis absorption, and Raman spectra, can be found on the producer's website (www.graphene-supermarket.com). Al_2O_3 substrates from Tesla (type KBI2) were used for MoS_2 flakes deposition. Each sensing substrate includes a Pt 1000 temperature sensor, heater, and platinum interdigitated electrodes structure (IDES) of line/gap width of 15/15 μm . More details on ceramic sensing substrates can be found on the producer's website (www.tesla-blatina.cz). Solution with MoS_2 flakes was first subjected to sonication for 30 min to ensure no aggregates. After that, Nordson Precision Fluid Dispenser (type Ultimius Plus II) was used to deposit ten layers of MoS_2 dispersion onto a cleaned ceramic substrate. After deposition of each layer, the material was dried in airflow ($\sim 50^\circ\text{C}$) to evaporate the residuals of ethanol solvent. Ten printing repetitions ensured that the randomly deposited, overlapping MoS_2 flakes provided the percolation network for electrical measurements. Supplementary Fig. S1 illustrates the deposition process, and Supplementary Table S1 summarizes the printing parameters.

Optical, structural, electrical, and noise measurements

UV-Vis spectroscopy of the MoS_2 flakes dispersion was realized using Evolution One Plus UV-Vis two-beam spectrophotometer (Thermo Scientific) with 1-nm wavelength resolution. Optical imaging of the material deposited on glass substrates was performed using a Delta Optical MET-1000-TRF microscope with up to 1000 \times magnification. For DC measurements, the IDES terminals were connected to the SMUs of the Keithley parameter analyzer (type 4200 A-SCS). Heater terminals were connected with the Keysight E3648A DC power supplier for experiments at an elevated temperature. Gas sensor current–voltage (I – V) characteristics were measured in the range of 0–20 V. Time-response and low-frequency noise measurements were conducted at 20 V. Noise spectra were collected with a signal analyzer (Stanford Research Systems, model SR785). The signal was amplified (1000 \times) using a low-noise voltage amplifier (Stanford Research Systems, model SR560). The sensing chamber, batteries, and voltage amplifier were put inside a grounded metal shielding box covered with an amorphous cobalt foil, type MCF5 YSHIELD, to reduce external noise interferences, the effect of ambient light, temperature changes, and laboratory airflow. Due to the high resistance of the MoS_2 sensor (at least tens



of $M\Omega$), voltage fluctuations were measured at the resistor R of lower resistance (478 k Ω) connected in series with the sensor. Further, these voltage fluctuations were converted into current fluctuations at the sensor R_S . Monitoring voltage at the resistor R enabled the calculation of the current flowing through the resistor R and the sensor R_S , which is necessary to normalize the power spectral density of current fluctuations $S_I(f)$ for further analysis. We analyzed noise spectra in the frequency range of 0.25–20 Hz collected with a resolution of 0.25 Hz. UV LED (275 nm, type PB2D-1CLA-TC) was positioned close to the sensing surface (less than 0.5 cm) for light-assisted measurements. Setting of the optical power density of the UV LED (0.40–1.59 mW/cm²) was obtained by adjusting the polarization current.

Gas-sensing experiments

The MoS₂ sensor was placed into the glass chamber for gas-sensing experiments and connected via the Teflon board with the measuring and biasing units to reduce leakage currents. Nitrogen dioxide (NO₂), ammonia (NH₃), and acetone (C₃H₆O) were used as target gases for the DC characteristics, time response, and low-frequency noise measurements. Each of the selected gases represents a different type of interaction with the semiconducting MoS₂. NO₂ is a strongly oxidizing agent, NH₃ is an electron-donating gas, and acetone is an organic, nucleophilic molecule. Dry synthetic air (S.A.) was used as a carrier gas and a reference atmosphere in our studies. To obtain selected concentrations of target gases, we mixed S.A. with calibrating gases (20 ppm of NO₂ diluted in N₂, 30 ppm of NH₃ diluted in N₂, or 40 ppm of C₃H₆O diluted in N₂) at specific proportions (e.g., to produce 10 ppm of NO₂, we mixed 25 mL/min of NO₂ and 25 mL/min of synthetic air, so as the overall gas flow would be kept at 50 mL/min (50 sccm)). We maintained a constant overall gas flow of 50 mL/min regulated by mass flow controllers, Analyt-MTC, model GFC17, calibrated by the producer to synthetic air as a reference gas. To produce a relative humidity of 40%, dry S.A. was transferred through a glass bubbler with deionized water before reaching the sensing chamber. Sensing experiments were conducted at room temperature (~25 °C) or 60 °C and ambient pressure (~1 bar).

Data post-processing and detection limit estimation

The sensor responses were presented as relative changes in the sensor resistance R_S in reference to the sensor resistance in the carrier gas (S.A.) R_0 via the relation: $S = (R_S - R_0)/R_0$. The sensor baseline, accompanied by the time drift, was approximated by the exponential function: $S = S_0 + ae^{bt}$, where S_0 , a , and b are constants, whereas S and t represent the sensor relative resistive responses and time, respectively, and subtracted from the experimental data. The detection limit (DL) was estimated based on S under selected conditions according to the procedure described elsewhere³¹. A third-order polynomial function was used to fit the experimental data points obtained for each target gas. The deviation between experimental and theoretical values of the sensor resistive response was used to estimate the root mean square (RMS). DL was determined using the formula: $DL = (S/N)\text{-RMS/slope}$, where $S/N = 3$ (signal-to-noise ratio). The slope was derived by fitting the quasi-linear region of each set of data points. Noise spectra were presented as the power spectral density of current fluctuations derived from voltage fluctuations measured at resistor R according to the relation: $S_I(f) = S_V(f)/R^2$.

Results and discussion

Structural and optical characterization of MoS₂ flakes

In our work, we study MoS₂ flakes with a size distribution of 100–400 nm (schematically depicted in Supplementary Fig. S2a). We utilize a ceramic sensing platform that provides temperature control and interdigitated electrodes (IDES) to connect with the printed MoS₂ layer (see Supplementary Fig. S2b). Figure 1 demonstrates the UV-Vis absorbance of the dispersion after 30 min of sonication to ensure its homogeneity. The absorbance of MoS₂ flakes was calculated in reference to ethanol solvent. Supplementary transmission spectra for the 300–1000 nm range for MoS₂ dispersion and ethanol can be found in Supplementary Fig. S3. Four principal local maxima are visible on the absorbance spectrum. Bands A (660 nm) and B (602 nm) represent excitonic transitions in the K point of the Brillouin zone characteristic for a few-layered MoS₂. The bands designated as C (387 nm) and D (323 nm) correspond to excitonic transitions in the regions of high density of states within the Brillouin zone³². The A band at 660 nm corresponds to the energy of ~1.9 eV ascribed to the direct optical bandgap in MoS₂. According to other reports on spectroscopic studies on MoS₂, the position of the A band can indicate the thickness of the MoS₂ layers, suggesting that MoS₂ flakes in the dispersion are mainly bilayers and monolayers in the case of our sensor³³. While the A and B doublet is associated with the optical properties of the MoS₂ independent from the lateral size of the structures, the C and D doublet characterizes the nanosized MoS₂ flakes, and its position can be blue-shifted with the decreasing size of the flakes. Moreover, relatively lower absorbance for the A–B than the C–D doublet can result from the low concentration of MoS₂ flakes in the solvent.

Transmission optical microscopic images of the MoS₂ film formed by ten repetitions of printing can be found in Supplementary Fig. S4. Optical imaging confirms the non-uniformity of the deposited structure in the microscale, with thicker parts and aggregates forming due to the simultaneous evaporation of the solvent and the outward flow of the droplet. This results in the coffee ring effect, a common phenomenon for ethanol-based solutions of low viscosity without any additives or binders²⁷. More detailed characterization of the MoS₂ flakes can be found elsewhere³⁴.

DC resistance measurements

Since UV light has been repeatedly reported to influence the conductance of the MoS₂ monolayers³⁵, we opted for a UV-C LED (maximum optical power at 275 nm) for light-assisted measurements. We started the electrical measurements by studying the effect of the optical power density of the UV light on the MoS₂ electrical characteristics. Figure 2a shows the current-voltage characteristics (I – V) of the MoS₂ sensor in synthetic air (S.A.) under UV irradiation of optical power density between 0.40 and 1.59 mW/cm². We kept the constant

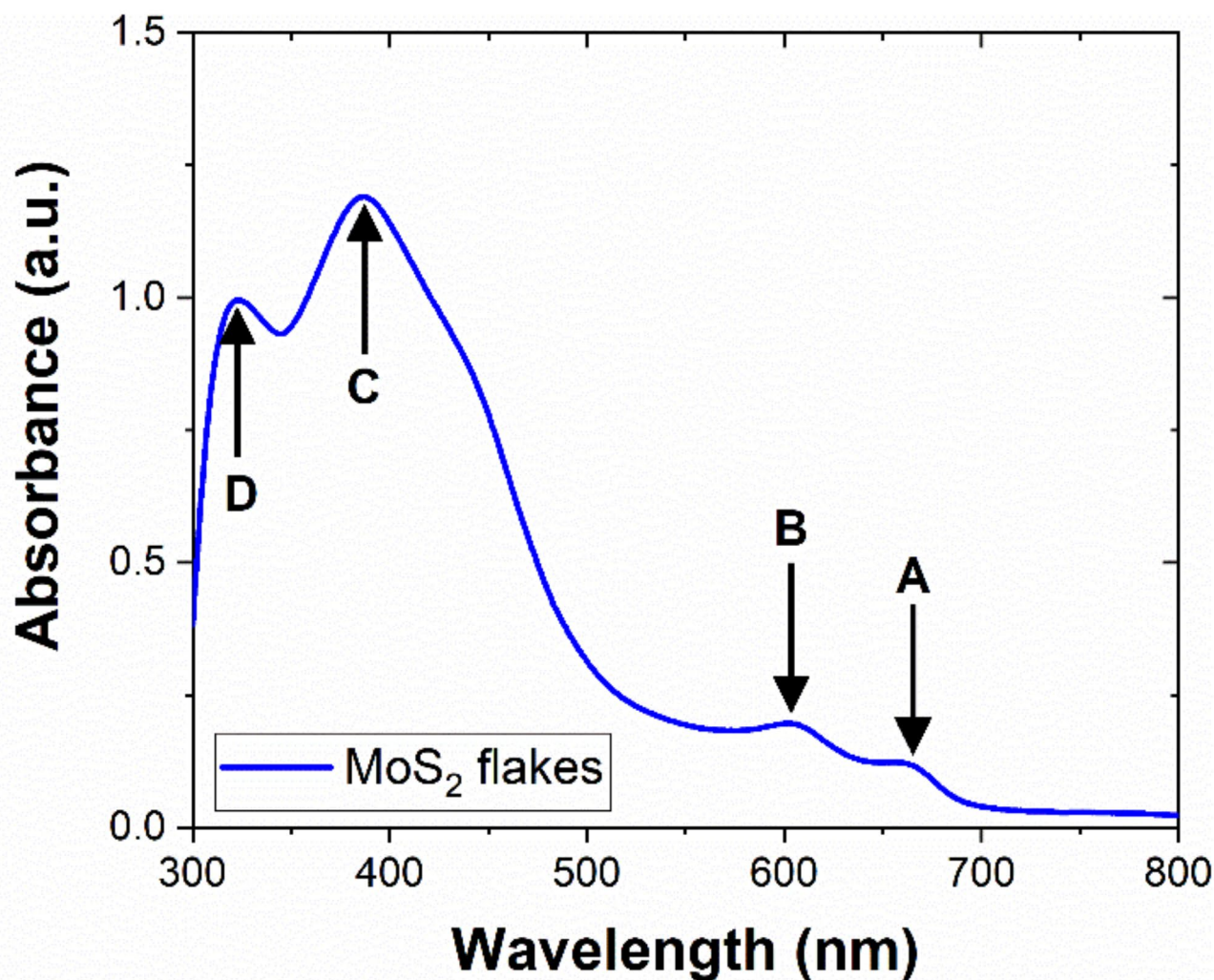


Fig. 1. UV-vis absorbance spectrum for MoS₂ flakes dispersion used for gas-sensitive layers printing. Letters A and B represent optical band transitions independent from the lateral dimensions of the MoS₂ flakes (660 nm and 602 nm). In contrast, letters C and D represent the excitonic bands ascribed to the nanosized sheets of MoS₂ (387 nm and 323 nm).

distance between the UV LED and the sensing surface (~ 0.5 cm) for these measurements. The maximum optical power density investigated was 1.59 mW/cm², which provided the most significant effect on the current flowing through the sensor and was selected for further UV-assisted experiments with target gases. Moreover, the I - V curve shows a deviation from the ohmic behavior in the 0–20 V range, which is expected for the structure consisting of multiple semiconducting nanoflakes overlapping each other and creating a percolation network. Figure 2b demonstrates the current response to four consecutive cycles of UV irradiation (275 nm, 1.59 mW/cm²) ON/OFF switching. We observed the constant time drift towards lower currents, but the relative change in the current (peak-to-peak values) due to irradiation was the same, i.e., between 18 and 20% in each cycle. The values were derived as $(I_{\text{ON}} - I_{\text{OFF}})/I_{\text{OFF}}$ where I_{ON} is the current flowing through the irradiated sensor (the last point from the considered irradiation cycle), and I_{OFF} is the current flowing through the dark sensor (the last point from the cycle in the dark)—see how the current responses were derived from Fig. 2 in Supplementary Material (Supplementary Fig. S5). Similar results were reported by Kumar et al. for the MoS₂ sensor, which exhibited $\sim 18\%$ stable response under UV irradiation¹⁷. The reason for the observed drift can be that printed MoS₂ is not a single atomic layer but is formed by multiple nanoflakes. Thus, the resistance of individual flakes and the structure boundaries contribute to the overall sensor resistance. Applying higher voltage and inducing photocurrent in the structure might cause the elongated stabilization process, mainly when UV light activates surface cleaning by removing preadsorbed oxygen and humidity. Therefore, ink-printed MoS₂ layers may exhibit longer photocurrent relaxation and less pronounced saturation in the air compared to individual atomically thin flakes³⁶.

Before gas sensing experiments, we cleaned the sensor surface for approximately one hour under UV irradiation in S.A. to reduce the short-time drift and stabilize the baseline to some extent. We started gas sensing experiments with nitrogen dioxide (NO₂), representing the inorganic oxidizing species harmful to the

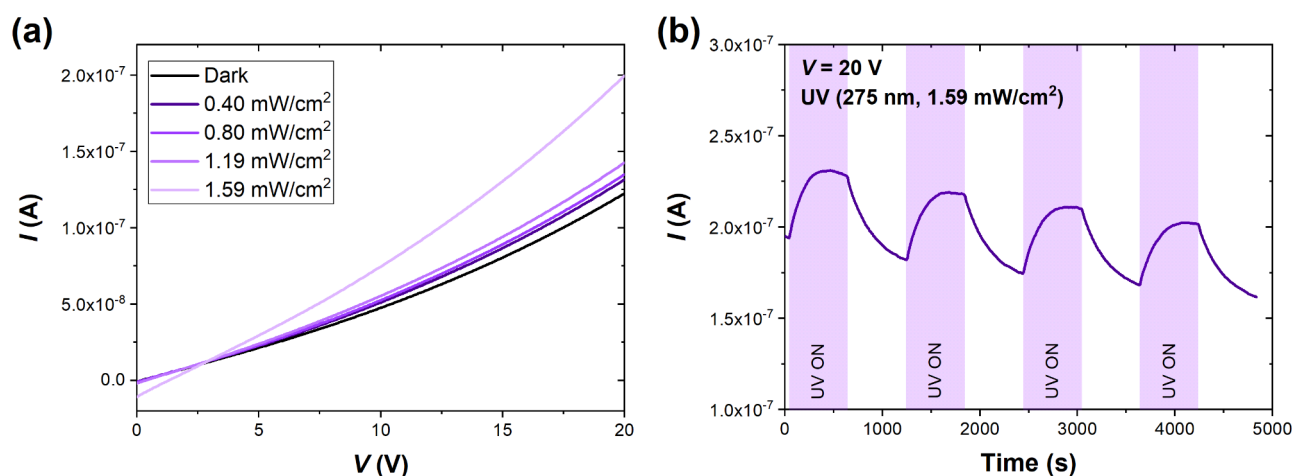


Fig. 2. (a) Current–voltage (I – V) characteristics of MoS_2 sensor in S.A. for different optical power densities of the UV LED (275 nm), and (b) time response (current) of MoS_2 sensor to four consecutive cycles of UV light (275 nm, 1.59 mW/cm^2) irradiation. Each irradiation cycle lasted 10 min, followed by 10 min of recovery in the dark. The bias voltage was set to 20 V for time-response measurements.

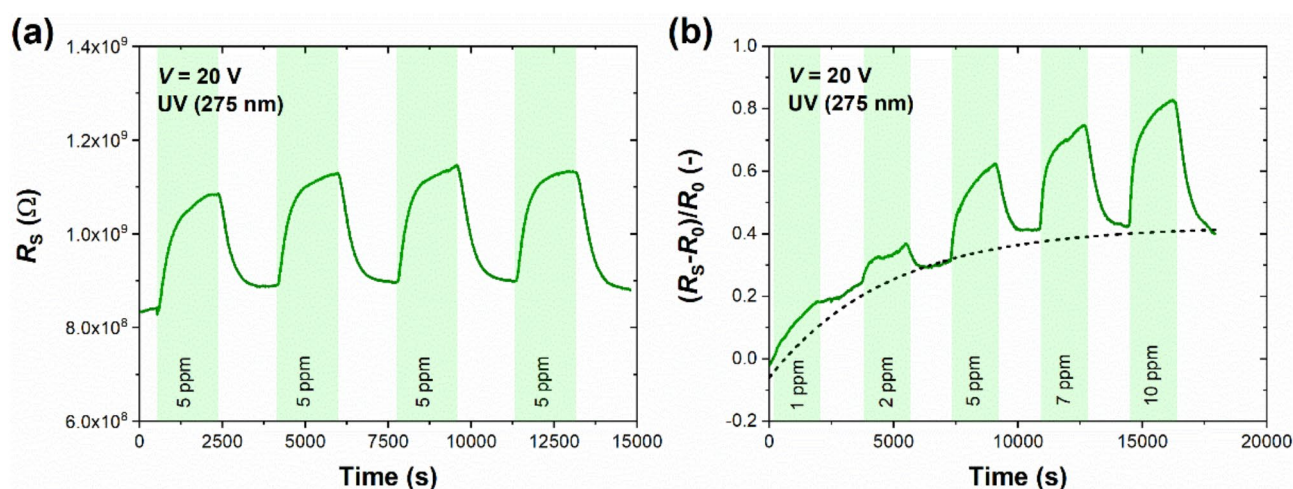


Fig. 3. (a) Time response (resistance) of MoS_2 sensor to four consecutive cycles of NO_2 (5 ppm) introduction; and (b) time response (relative changes in resistance) of MoS_2 sensor to five cycles of NO_2 of selected concentrations (1–10 ppm) under UV light (275 nm). Each detection cycle consisted of 30 min-response and 30 min-recovery in S.A. The bias voltage was set to 20 V. The black dashed exponential curve in (b) denotes the time drift present during detection.

environment and humans even at the ppb-concentration level³⁷. Although NO_2 usually bonds strongly with the sensing surfaces of nanomaterials via physical forces, room-temperature sensing usually requires an additional boost to maximize the sensitivity toward the gas and minimize the detection limit. UV light successfully fulfilled these requirements for graphene and MoS_2 sensors^{38–40}. Figure 3 summarizes the qualitative and quantitative detection of NO_2 by printed MoS_2 sensor. Consecutive cycles of introducing 5 ppm NO_2 resulted in repeatable responses (the average peak-to-peak resistive response of $\sim 28\%$) with time drift reduced after the first detection cycle (Fig. 3a). For quantitative detection, the sensor was subjected to NO_2 concentrations between 1 and 10 ppm. Figure 3b presents the relative changes in the sensor resistance R_s in reference to resistance in S.A. NO_2 increases the sensor resistance, which agrees with the oxidizing nature of NO_2 interacting with the n -type semiconductor. When NO_2 molecules adsorb on the MoS_2 surface, they extract electrons and reduce the number of majority carriers in the sensing material, resulting in higher resistance. UV excitation provides additional light-generated electrons that may participate in molecular detection but also increases the probability of adsorption by cleaning the binding sites occupied by the oxygen and humidity species from the atmospheric air. It can also be noticed that sensing smaller concentrations of NO_2 (1 and 2 ppm) is subjected to more intense time drift. We observed that the sensor responded reproducibly when the experiment was repeated in the following days after staying in laboratory air during the night, necessary for its full recovery. Similar drift components were observed

elsewhere⁴¹. As the baseline drift of the MoS₂ sensor was observed to diminish in time, suggesting the process with a particular relaxation time, it was fitted to the exponential function described in Methods. The processed data represents the actual responses to the target gas without the influence of the drifting baseline. The results of the data processing for NO₂ are depicted in Supplementary Fig. S6. Another ink-printed MoS₂ sensor was also tested toward NO₂ (5 ppm) in the dark and under UV light (see Supplementary Fig. S7). Resistive response in the dark was only 4% but reached ~20% under UV light for 15-min exposure to NO₂ (at V=20 V). This observation confirmed the superiority of UV-assisted sensing; therefore, we continued with UV light sensing only in all following experiments.

Figure 4 shows the effect of ammonia (NH₃) on the studied device. The repeatable resistance decrease toward 5 ppm of NH₃ can be visible in Fig. 4a. Ammonia is a reducing gas with a lone-pair electron acting as an electron donor to MoS₂. Similarly to the NO₂ case, a substantial time drift, particularly in low concentrations of NH₃ (2 and 5 ppm), is visible in Fig. 4b. The stabilized sensing response is visible for 7 ppm and higher concentrations, where the sensor responsivity is much stronger. The resistive responses to 2–12 ppm NH₃ after data processing and subtracting the drifting baseline are depicted in Supplementary Fig. S8. Here, the decreasing resistance toward subsequent cycles of NH₃ detection is much more apparent and simplifies the interpretation of the direction of changes in MoS₂ electrical properties after the adsorption of the reducing gas.

A similar reduction of the sensor resistance was observed during acetone (C₃H₆O) detection. Usually, organic vapors bind weakly with the surfaces of low-dimensional materials and exhibit relatively low adsorption energies^{42,43}. Figure 5a shows repeatable cycles of 5 ppm acetone introduction under continuous UV irradiation, and Fig. 5b demonstrates the sensor responsivity toward increasing acetone concentration (2–12 ppm). Both measurements are accompanied by time drift, which is more pronounced than for NO₂ and NH₃ cases. After fitting and subtracting the drifting baseline (see Supplementary Fig. S9), one can notice that acetone exhibits reducing properties during interaction with the MoS₂ surface, similar to ammonia. Comparing the same concentration range for both reducing gases, we can observe that inorganic ammonia produces higher and more stable responses in each detection cycle than organic acetone. Nevertheless, the resistive responses reach up to ~20% for 12 ppm of acetone, and the obtained results are higher than reported before for pure MoS₂ under UV light at RT⁴⁴. Based on the DC response studies, we can see that the sensor responsivity is superior to oxidizing NO₂ rather than to reducing gases (see Supplementary Fig. S10 illustrating the sensor selectivity based on the time-resolved resistance monitoring). In terms of response and recovery times, there is no strict correlation with the type or concentration of gas, as shown in Supplementary Fig. S11, and time constants are at least in the several-minute range. Additionally, introducing relative humidity (RH) of 40% during sensing of 5 ppm of NO₂, NH₃, and C₃H₆O showed that resistive responses were slightly increased in a humid atmosphere. However, in dry S.A., the sensor maintained its responsivity toward selected target gases after four months of storage in laboratory air conditions. The results showing the sensor stability and the effect of RH=40% are presented in Supplementary Table S2 and Supplementary Fig. S12.

Another crucial figure of merit for a gas sensor is the detection limit (DL), which informs about the maximum sensitivity to a specific target gas. Here, DL was estimated before and after subtracting the baseline drift to see if post-processing of detection data improves DL for the MoS₂ sensor. Figure 6 compares DL values for NO₂, NH₃, and C₃H₆O calculated based on relative resistive responses $(R_s - R_0)/R_0$ according to the procedure described in Methods. The authors designated the pre-processed and post-processed data points as the “drift” and “subtracted drift” cases. For the drift case, the response data measured for the lowest concentration of each gas (1 ppm for NO₂ and 2 ppm for NH₃ and C₃H₆O) was purposely omitted as these points were the least

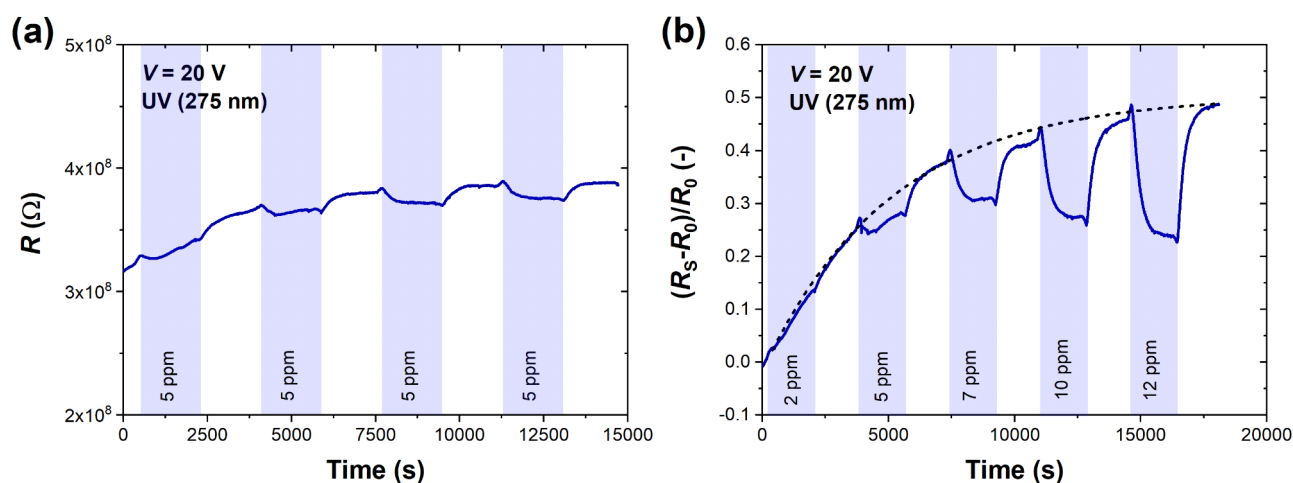


Fig. 4. (a) Time response (resistance) of MoS₂ sensor to four consecutive cycles of NH₃ (5 ppm) introduction; and (b) time response (relative changes in resistance) of MoS₂ sensor to five cycles of NH₃ of selected concentrations (2–12 ppm) under UV light (275 nm). Each detection cycle consisted of 30 min-response and 30 min-recovery in S.A. The bias voltage was set to 20 V. The black dashed exponential curve in (b) denotes the time drift present during detection.

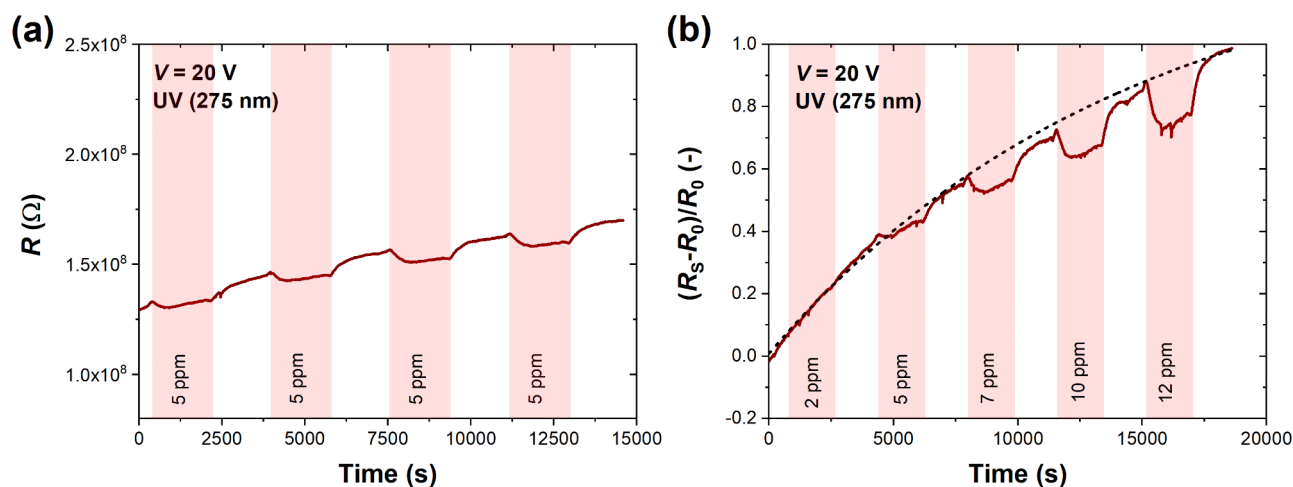


Fig. 5. (a) Time response (resistance) of MoS_2 sensor to four consecutive cycles of C_3H_6O (5 ppm) introduction; and (b) time response (relative changes in resistance) of MoS_2 sensor to five cycles of C_3H_6O of selected concentrations (2–12 ppm) under UV light (275 nm). Each detection cycle consisted of 30 min-response and 30 min-recovery in S.A. The bias voltage was set to 20 V. The black dashed exponential curve in (b) denotes the time drift present during detection.

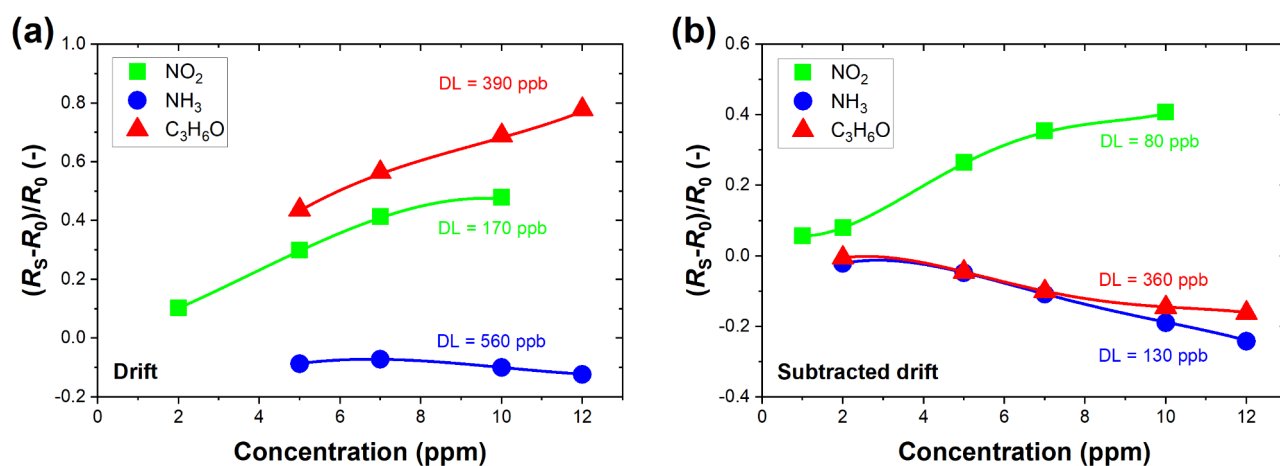


Fig. 6. Relative changes in MoS_2 sensor resistance as a function of target gas concentration for NO_2 , NH_3 , and C_3H_6O under UV light (275 nm) (a) before and (b) after subtraction of the drift baseline. Theoretical detection limits established for NO_2 , NH_3 , and C_3H_6O are marked on the graphs and are equal to 170 ppb, 560 ppb, 390 ppb (drift case), and 80 ppb, 130 ppb, and 360 ppb (subtracted drift case), respectively. Solid curves correspond to a third-order polynomial function fitted to the experimental points for DL estimation. The responses to acetone burden with drift do not show the real direction of changes in sensor resistance.

readable out of the drifting baseline, making the DL analysis much less reliable. Indeed, the time drift influences the sensing responses. If the target gas increases the sensor resistance (oxidizing NO_2), the post-processed data points reveal slightly lower responses. On the other hand, if the gases decrease the sensor resistance (reducing NH_3 and acetone), their responses become more pronounced and readable, constituting a much more reliable representation of the actual adsorption process and direction of charge transfer occurring between MoS_2 flakes and target gases. Despite the drifting baseline, Fig. 6a demonstrates that all three gases exhibit sub-ppm DL, with the lowest value of 170 ppb obtained for NO_2 . However, due to the substantial time drift and weakly binding gas molecules, the DL values calculated for reducing gases are burdened with a significant error, particularly for acetone. Hence, the “subtracted drift” case presents more reliable results (Fig. 6b). DL values calculated after data processing are 80 ppb, 130 ppb, and 360 ppb for NO_2 , NH_3 , and C_3H_6O , respectively. This means that for NO_2 and NH_3 , the DL was improved more than 2 and 4 times, respectively, only by simple data post-processing. This suggests an easy method of improving the performance of sensors based on solution-processed, ink-printed MoS_2 flakes. The DL estimated for NO_2 and NH_3 falls significantly beyond the maximum permissible limits set by the European Union, which are 0.5 ppm and 1 ppm for 8-h and 15-min exposure for NO_2 , and 20 ppm and

50 ppm for the long and short exposure for NH_3 ⁴⁵. Up to the authors' knowledge, in the case of acetone, the sub-ppm limit was reached only at elevated temperatures (0.1 ppm at 300 °C–100 °C with additional UV irradiation), and it was reported for HZnO/MoS₂ hybrid sensors⁴⁴. For pure MoS₂, the DL for acetone reaching lower than 0.9 ppm still requires further investigation¹, making our proposed sensor promising for the efficient detection of this organic gas.

To fulfill the investigation on possible methods of improvement of sensitivity for printed MoS₂ sensors, measurements at an elevated temperature (60 °C) were performed for all three target gases. Interestingly, the elevated temperature did not improve the MoS₂ sensor performance. On the contrary, only an unstable drift upwards was observed for 5 ppm of NO₂, NH₃, and acetone (see Supplementary Fig. S13 for time responses under 60 °C and UV irradiation and proposed explanation for this observation).

Low-frequency noise measurements

Fluctuation-enhanced sensing was another method to investigate the sensing performance of the UV-assisted MoS₂ sensor. Low-frequency noise was measured and analyzed up to 20 Hz, where the $1/f$ noise was observed to be the dominant noise component over background and white noise. Noise spectra were collected for different concentrations of NO₂, NH₃, and C₃H₆O that corresponded to the DC measurements and are depicted in Fig. 7. The adsorption of oxidizing NO₂ decreases the normalized current noise power spectrum $S_I(f)/I^2$ with the gas concentration increase. Such direction of sensor responses correlates with the decrease in the current flowing through the sensor caused by NO₂. The opposite effect can be observed for ammonia since higher concentrations of NH₃ visibly increase the current fluctuations. In the case of the organic acetone, the noise responses to this gas are minor, even for the highest concentrations investigated. The results indicate that the adsorption of only some gases of the considered low concentrations induces distinct fluctuations, and the FES method can be used for determining the concentration of NO₂ and NH₃. However, the range of concentrations can be limited and differ for various gases, e.g., 1 ppm of NO₂ and 2 ppm of NH₃ produce only minor changes in the noise intensity. Additionally, Fig. 7d demonstrates the magnitude of the relative changes introduced in the noise of the MoS₂ sensor. Based on these results, it is easy to distinguish between oxidizing and reducing gas (NO₂ and NH₃) due to the opposite direction of responses. The noise response to NO₂ saturates from 7 ppm, reaching around -0.6 . On

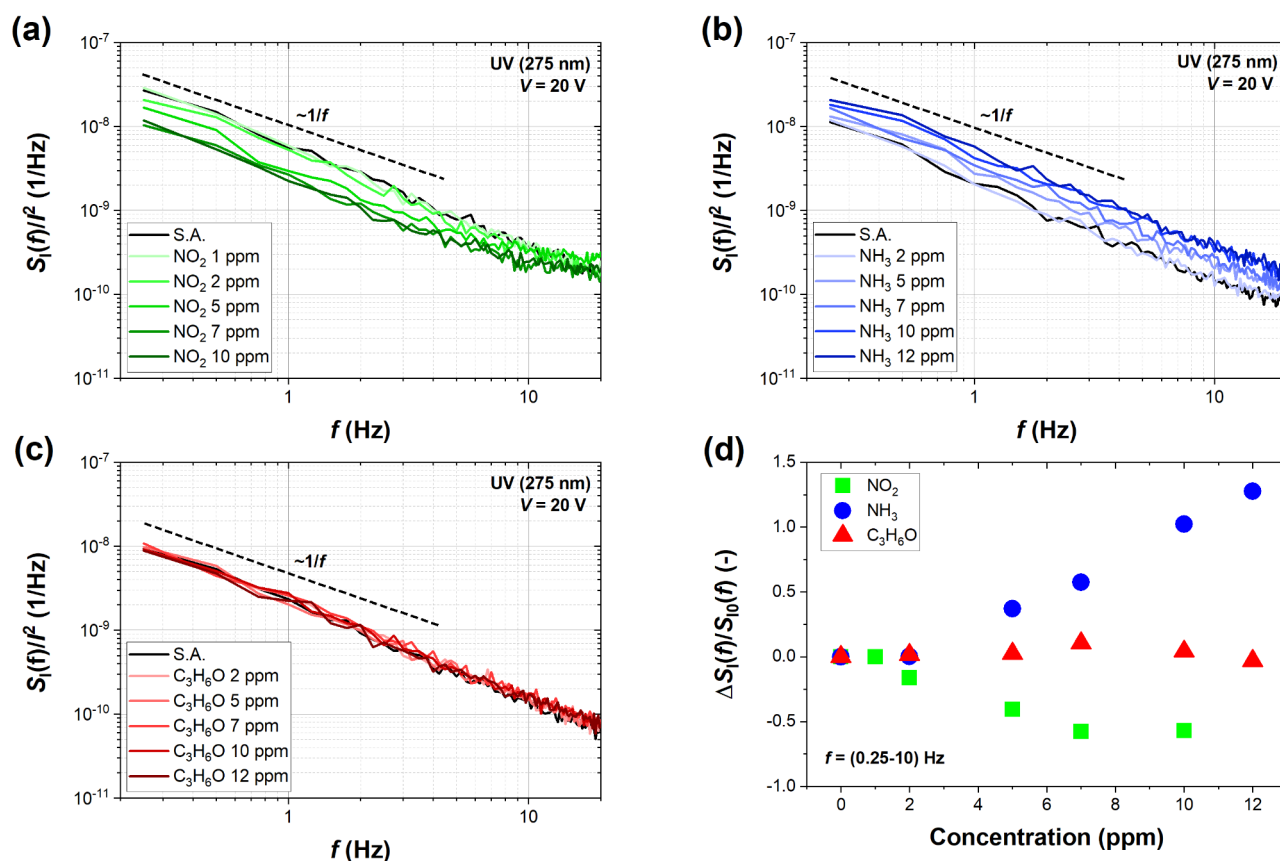


Fig. 7. Power spectral density of current fluctuations $S_I(f)$ normalized to the squared bias current I^2 for selected concentrations of (a) NO₂, (b) NH₃, and (c) C₃H₆O. The dashed lines correspond to the $1/f$ noise dependence. The spectra were measured under UV light (275 nm) at voltage bias $V = 20$ V across the sensor. Data points in (d) correspond to the relative changes $\Delta S_I(f)/S_{I0}(f)$ in the noise current power spectral density in the target gas of selected concentration $\Delta S_I(f) = S_I(f) - S_{I0}(f)$ in relation to the reference case of S.A. $S_{I0}(f)$ (the values are averaged for frequencies 0.25–10 Hz).

the contrary, noise amplitude increases proportionally, with NH_3 concentration reaching ~ 1.3 , showing a high linearity of sensor responsivity. The saturation for NH_3 is likely to be achieved for much higher concentrations, whereas in the case of NO_2 , FES can be utilized efficiently toward the range of lower concentrations (below 7 ppm). In the case of acetone, no relevant changes in the noise intensity suggest that such low concentrations of this gas cannot be detected with sufficient accuracy based on the $1/f$ noise spectra. Interestingly, the sensitivity of noise spectra to higher concentrations of acetone (110 ppm) and other organic vapors was reported recently for the ink-printed MoS_2 , suggesting that organic species can produce distinct noise spectra but at much higher concentrations¹⁸. It can be explained by their low binding energies (adsorption energies) to different types of materials and limited charge transfer, which is the primary mechanism of gas detection by 2D semiconducting metal sulfides. Moreover, noise responses for NO_2 and NH_3 are higher than DC resistance responses with subtracted drift baseline. For instance, 10 ppm of NO_2 induces the absolute value of resistive response of ~ 0.4 and noise response of ~ 0.6 , an increase of 50%. For 12 ppm of NH_3 , this increase is even more apparent as the noise response is more than six times higher (~ 1.3) than the resistive response (~ 0.2). At the same time, the adsorption of NO_2 and NH_3 does not induce any characteristic events in the form of Lorentzians dominant over the $1/f$ noise spectrum, as was observed for graphene-based sensors²⁰. Moreover, it was previously confirmed that low-frequency noise spectra of monolayers and bilayers of MoS_2 respond poorly to selected organic vapors (e.g., ethanol, methanol, toluene), and the increased noise intensity was observed only to acetonitrile⁴⁶. However, no quantitative sensing has been reported for this material, specifically for ink-printed light-assisted MoS_2 . This makes room for original research and discoveries, and our results pave the way toward novel applications for this type of materials and the FES method.

Conclusions

MoS_2 sensors were fabricated employing the ink-printing of nanosized flakes dispersed in an ethanol-water solution. The optical characterization of the dispersion revealed that it primarily consists of bilayered and monolayered MoS_2 with direct optical bandgap in the red-light region of the spectrum (660 nm). The optical imaging confirmed that the printed structure is formed with sub- μm flakes, non-uniformly deposited on the ceramic substrate. Despite the coffee-ring effect, the size of the deposited droplets larger than the IDES area provided a uniform distribution of flakes and reduced aggregation of the material (compared to the edges of the droplet) in the region of interest for electrical and low-frequency noise measurements. Printing repetitions and deposition of the 10-layered structure ensured the percolation path between nanoflakes printed onto a ceramic platform with platinum electrodes of 15 μm -gap for electrical measurements. The deposited MoS_2 structure exhibited $\sim 10^8 \Omega$ resistance at the biasing voltage of 20 V and under UV irradiation (275 nm, 1.59 mW/cm²). The UV light ensured stable current flow through the sensor; however, it did not completely diminish the short-time drift of the sensor resistance. The drifting baseline specifically affected the detection of reducing gases (ammonia and acetone) and disturbed the interpretation of the direction of changes introduced by these species. Data post-processing and subtraction of the drifting baseline enabled the reduction of the detection limit to 80 ppb, 130 ppb, and 360 ppb for NO_2 , NH_3 , and $\text{C}_3\text{H}_6\text{O}$, respectively, showing the possibility of enhancing sensitivity for printed MoS_2 gas sensors at RT. In compliance with the redox properties of target gases, NO_2 increased the sensor resistance, whereas NH_3 and acetone reduced it, confirming the *n*-type conductivity of the MoS_2 structure. Low-frequency noise measurements reveal that FES can be utilized to determine the concentration of NO_2 and NH_3 for the linear range of the changes induced in the noise amplitude (below 7 ppm for NO_2 and up to 12 ppm of NH_3). Supplementary Table S3 summarizes the properties of MoS_2 -based gas sensors operating at RT and utilizing UV light assistance reported recently, showing that ink-printed MoS_2 sensor offers simplicity of its fabrication while still preserving the high sensitivity and selectivity increased with the FES method. Combining DC resistance measurements with the FES has the potential to become a highly sensitive tool for light-assisted gas detection by ink-printed MoS_2 and similar structures.

Data availability

The detailed data that support the findings of our experimental study are available from the corresponding author upon reasonable request.

Received: 19 July 2024; Accepted: 18 September 2024

Published online: 27 September 2024

References

1. Tang, H. et al. Recent advances in 2D/nanostructured metal sulfide-based gas sensors: mechanisms, applications, and perspectives. *J. Mater. Chem. A*. **8**, 24943–24976 (2020).
2. Zhao, P. X. et al. One-dimensional MoS_2 -Decorated TiO_2 nanotube gas sensors for efficient alcohol sensing. *J. Alloys Compd.* **674**, 252–258 (2016).
3. Burman, D., Ghosh, R., Santra, S. & Kumar Ray, S. & Kumar Guha, P. Role of vacancy sites and UV-ozone treatment on few layered MoS_2 nanoflakes for toxic gas detection. *Nanotechnology* **28**, (2017).
4. Tian, X. et al. Recent advances in MoS_2 -based nanomaterial sensors for room-temperature gas detection: a review. *Sens. Diagn.* **2**, 361–381 (2023).
5. Donarelli, M. & Ottaviano, L. 2D materials for gas sensing applications: a review on graphene oxide, MoS_2 , WS_2 and phosphorene. *Sens. (Switzerland)* **18**, (2018).
6. Pham, T., Li, G., Bekyarova, E., Itkis, M. E. & Mulchandani, A. MoS_2 -based optoelectronic gas sensor with sub-parts-per-billion limit of NO_2 gas detection. *ACS Nano*. **13**, 3196–3205 (2019).
7. Kumar, R., Zheng, W., Liu, X., Zhang, J. & Kumar, M. MoS_2 -based nanomaterials for room-temperature gas sensors. *Adv. Mater. Technol.* **5**, 1–28 (2020).
8. Cho, B. et al. Charge-transfer-based gas sensing using atomic-layer MoS_2 . *Sci. Rep.* **5**, 1–6 (2015).

9. Zhao, H. et al. Oxygen vacancy-rich bimetallic Au@Pt core-shell nanosphere-functionalized electrospun ZnFe₂O₄ nanofibers for chemiresistive breath acetone detection. *ACS Sens.* **9**, 2183–2193 (2024).
10. Zhao, H. et al. Black phosphorus nanosheets-sensitized Zn-doped α -Fe₂O₃ nanoclusters for trace acetone detection. *Sens. Actuators B-Chem.* **395**, 134496 (2023).
11. Zhao, H. et al. Black phosphorus nanosheets decorated Multiscale Zinc Ferrite spheres toward swift and humidity-tolerant breath acetone sensing. *IEEE Sens. J.* **23**, 1908–1916 (2023).
12. Joshi, N. et al. A review on chemiresistive room temperature gas sensors based on metal oxide nanostructures, graphene and 2D transition metal dichalcogenides. *Microchim Acta.* **185**, 1–16 (2018).
13. Zhang, J., Liu, X. & Neri, G. Pinna N. Nanostructured materials for room-temperature gas sensors. *Adv. Mater.* **28**, 795–831 (2016).
14. Zhou, Y., Zou, C., Lin, X. & Guo, Y. UV light activated NO₂ gas sensing based on au nanoparticles decorated few-layer MoS₂ thin film at room temperature. *Appl. Phys. Lett.* **113** (2018).
15. Zhou, Y., Gao, C. & Guo, Y. UV assisted ultrasensitive trace NO₂ gas sensing based on few-layer MoS₂ nanosheet-ZnO nanowire heterojunctions at room temperature. *J. Mater. Chem. A.* **6**, 10286–10296 (2018).
16. Ramu, S. et al. UV enhanced NO gas sensing properties of the MoS₂ monolayer gas sensor. *Mater. Res. Express* **6**, (2019).
17. Kumar, R., Goel, N. & Kumar, M. UV-activated MoS₂ based fast and reversible NO₂ sensor at room temperature. *ACS Sens.* **2**, 1744–1752 (2017).
18. Drozdowska, K., Smulko, J., Rummyantsev, S. & Kwiatkowski, A. Fluctuation-enhanced sensing of organic vapors by Ink-printed MoS₂ devices under UV irradiation. in *2024 IEEE International Instrumentation and Measurement Technology Conference (I2MTC) 1–5* (IEEE, 2024).
19. Balandin, A. A. Low-frequency 1/f noise in graphene devices. *Nat. Nanotechnol.* **8**, 549–555 (2013).
20. Drozdowska, K. et al. Organic Vapor sensing mechanisms by large-area Graphene back-gated field-effect transistors under UV irradiation. *ACS Sens.* <https://doi.org/10.1021/acssensors.2c01511> (2022).
21. Drozdowska, K. et al. Effects of UV light irradiation on fluctuation enhanced gas sensing by carbon nanotube networks. *Sens. Actuators B Chem.* **352**, 131069 (2022).
22. Kish, L. B. B., Vajtai, R. & Granqvist, C. G. Extracting information from noise spectra of chemical sensors: single sensor electronic noses and tongues. *Sens. Actuators B-Chem.* **71**, 55–59 (2000).
23. Aroutiounian, V. M. et al. Noise spectroscopy of gas sensors. *IEEE Sens. J.* **8**, 786–790 (2008).
24. Rummyantsev, S., Liu, G., Shur, M. S., Potyralo, R. A. & Balandin, A. A. Selective gas sensing with a single pristine graphene transistor. *Nano Lett.* **12**, 2294–2298 (2012).
25. Tabata, H., Matsuyama, H., Goto, T., Kubo, O. & Katayama, M. Visible-light-activated response originating from carrier-mobility modulation of NO₂ gas sensors based on MoS₂ monolayers. *ACS Nano.* **15**, 2542–2553 (2021).
26. Espid, E. & Taghipour, F. UV-LED photo-activated chemical gas sensors: a review. *Crit. Rev. Solid State Mater. Sci.* **42**, 416–432 (2017).
27. Hu, G. et al. Functional inks and printing of two-dimensional materials. *Chem. Soc. Rev.* **47**, 3265–3300 (2018).
28. Dai, J. et al. Printed gas sensors. *Chem. Soc. Rev.* **49**, 1756 (2020).
29. Yao, Y. et al. High-concentration aqueous dispersions of MoS₂. *Adv. Funct. Mater.* **23**, 3577–3583 (2013).
30. Chen, M. et al. Inkjet-printed MoS₂ nanoplates on flexible substrates for high-performance field effect transistors and gas sensing applications. *ACS Appl. Nano Mater.* **6**, 3236–3244 (2023).
31. Chen, G., Paronyan, T. M., Pigos, E. M. & Harutyunyan, A. R. Enhanced gas sensing in pristine carbon nanotubes under continuous ultraviolet light illumination. *Sci. Rep.* **2**, (2012).
32. Ghayeb Zamharir, S., Karimzadeh, R. & Aboutalebi, S. H. Laser-assisted tunable optical nonlinearity in liquid-phase exfoliated MoS₂ dispersion. *Appl. Phys. Mater. Sci. Process.* **124**, 1–8 (2018).
33. Wang, Q. H., Kalantar-Zadeh, K., Kis, A., Coleman, J. N. & Strano, M. S. Electronics and optoelectronics of two-dimensional transition metal dichalcogenides. *Nat. Nanotechnol.* **7**, 699–712 (2012).
34. Molybdenum Disulfide (MoS₂) Pristine Flakes in Solution, 100 ml. https://www.graphene-supermarket.com/products/molybdenum-disulfide-mos2-pristine-flakes-in-solution-100-ml?_pos=1&_sid=9fa89e206&_ss=r. (accessed 19.07.24).
35. Tian, X. et al. Recent advances in MoS₂-based nanomaterial sensors for room-temperature gas detection: a review. *Sens. Diagn.* **2**, 361–381 (2023).
36. Khan, M. F. et al. Photocurrent response of MoS₂ field-effect transistor by deep ultraviolet light in atmospheric and N₂ gas environments. *ACS Appl. Mater. Interfaces.* **6**, 21645–21651 (2014).
37. Fine, G. F., Cavanagh, L. M., Afonja, A. & Binions, R. Metal oxide semiconductor gas sensors in environmental monitoring. *Sensors.* **10**, 5469–5502 (2010).
38. Yan, X. et al. High-performance UV-assisted NO₂ sensor based on chemical vapor deposition graphene at room temperature. *ACS Omega.* **4**, 14179–14187 (2019).
39. Park, J. et al. UV illumination as a method to improve the performance of gas sensors based on graphene field-effect transistors. *ACS Sens.* **6**, 4417–4424 (2021).
40. Agrawal, A. V. et al. Photoactivated mixed In-Plane and edge-enriched p-Type MoS₂ flake-based NO₂ sensor working at room temperature. *ACS Sens.* **3**, 998–1004 (2018).
41. Bag, A., Bin Moon, D., Park, K. H., Cho, C. Y. & Lee, N. E. Room-temperature-operated fast and reversible vertical-heterostructure-diode gas sensor composed of reduced graphene oxide and AlGaIn/GaN. *Sens. Actuators B Chem.* **296** (2019).
42. Ganji, M. D., Mazaheri, H. & Khosravi, A. Acetone adsorption on pristine and Pt-doped graphene: a first-principles vdW-DF study. *Commun. Theor. Phys.* **64**, 576–582 (2015).
43. Lazar, P. et al. Adsorption of small organic molecules on graphene. *J. Am. Chem. Soc.* **135**, 6372–6377 (2013).
44. Chang, X. et al. UV assisted ppb-level acetone detection based on hollow ZnO/MoS₂ nanosheets core/shell heterostructures at low temperature. *Sens. Actuators B Chem.* **317**, 128208 (2020).
45. Buckley, D. J. et al. Frontiers of graphene and 2D material-based gas sensors for environmental monitoring. *2D Mater.* **7**, 1–48 (2019).
46. Samnakay, R., Jiang, C., Rummyantsev, S. L., Shur, M. S. & Balandin, A. A. Selective chemical vapor sensing with few-layer MoS₂ thin-film transistors: comparison with graphene devices. *Appl. Phys. Lett.* **106**, 1–6 (2015).

Acknowledgements

This work was funded by the National Science Centre, Poland under the research project: 2019/35/B/ST7/02370, “System of gas detection by two-dimensional materials”. S. R. acknowledges partial support by the CENTERA Laboratories under the European Regional Development Fund (No. MAB/2018/9) and by the European Union ERC “TERAPLASM” project No. 101053716. We would also like to thank Professor Marek Maryański for providing research equipment for optical measurements.

Author contributions

K.D.: Formal analysis, investigation, resources, data curation, writing—original draft, writing—review and editing, visualization. J.S.: Conceptualization, formal analysis, writing—review and editing, supervision. J.C.: Formal analysis, investigation, resources, writing—review and editing. S.R.: Formal analysis, writing—review and editing. A.K.: Writing—review and editing.

Declarations

Competing interests

The authors declare no competing interests.

Additional information

Supplementary Information The online version contains supplementary material available at <https://doi.org/10.1038/s41598-024-73525-2>.

Correspondence and requests for materials should be addressed to K.D.

Reprints and permissions information is available at www.nature.com/reprints.

Publisher's note Springer Nature remains neutral with regard to jurisdictional claims in published maps and institutional affiliations.

Open Access This article is licensed under a Creative Commons Attribution 4.0 International License, which permits use, sharing, adaptation, distribution and reproduction in any medium or format, as long as you give appropriate credit to the original author(s) and the source, provide a link to the Creative Commons licence, and indicate if changes were made. The images or other third party material in this article are included in the article's Creative Commons licence, unless indicated otherwise in a credit line to the material. If material is not included in the article's Creative Commons licence and your intended use is not permitted by statutory regulation or exceeds the permitted use, you will need to obtain permission directly from the copyright holder. To view a copy of this licence, visit <http://creativecommons.org/licenses/by/4.0/>.

© The Author(s) 2024